Materials Research Bulletin 63 (2015) 80–87

Contents lists available at ScienceDirect

Materials Research Bulletin

journal homepage: www.elsevier.com/locate/matresbu

Study of structural and optical properties of YAG and Nd:YAG single crystals

S. Kostić [a], Z.Ž. Lazarević [a,*], V. Radojević [b], A. Milutinović [a], M. Romčević [a], N.Ž. Romčević [a], A. Valčić [b]

[a] Institute of Physics, University of Belgrade, P.O. Box 68, Pregrevica 118, Zemun, Belgrade, Serbia
[b] Faculty of Technology and Metallurgy, University of Belgrade, Belgrade, Serbia

ARTICLE INFO

Article history:
Received 22 May 2014
Received in revised form 9 October 2014
Accepted 14 November 2014
Available online 18 November 2014

Keywords:
Single crystal
Nd:YAG
Optical materials
Crystal growth

ABSTRACT

Yttrium aluminum garnet (YAG, $Y_3Al_5O_{12}$) and yttrium aluminum garnet doped with neodymium (Nd:YAG) single crystals were grown by the Czochralski technique. The critical diameter and the critical rate of rotation were calculated. Suitable polishing and etching solutions were determined. As a result of our experiments, the transparent YAG and pale pink Nd:YAG single crystals were produced. The obtained crystals were studied by X-ray diffraction, Raman and IR spectroscopy. The crystal structure was confirmed by XRD. The 15 Raman and 17 IR modes were observed. The Raman and IR spectroscopy results are in accordance with X-ray diffraction analysis. The obtained YAG and Nd:YAG single crystals were without core and of good optical quality. The absence of a core was confirmed by viewing polished crystal slices. Also, it is important to emphasize that the obtained Nd:YAG single crystal has a concentration of 0.8 wt.% Nd^{3+} that is characteristic for laser materials.

1. Introduction

Oxide materials are very interesting and they are being used more and more. They are used as laser materials, in nonlinear optics, acousto optics, for memorizing optical data and magnetic memories, wave guides, etc. [1,2].

Yttrium aluminum garnet (YAG, $Y_3Al_5O_{12}$) and yttrium aluminum garnet doped with neodymium (Nd:YAG) are the most famous kind of oxide crystals widely used as the active medium in solid state lasers [3,4]. The dopant, triply ionized neodymium, Nd (III), typically replaces a small fraction of the yttrium ions in the host crystal structure of the yttrium aluminum garnet. It is the neodymium ion which provides the leasing activity in the crystal. Nd:YAG lasers typically emit light with a wavelength of 1064 nm, in the infrared. However, there are also transitions near 940, 1120, 1320, and 1440 nm. Nd:YAG lasers operate in both pulsed and continuous mode. Nd:YAG crystals are usually grown by the conventional Czochralski (CZ) technique [5–7]. Besides that, for miniature laser sources Nd:YAG can by the micro-pulling-down technique and by the crucibles laser heating pedestal method [8].

The Czochralski technique has great advantages for growth of the high quality and large size YAG and Nd:YAG single crystals for usage as medium – in high power efficient lasers. A stable and equilibrant process of crystal growth with CZ technique is necessarily controlled by many different growth parameters. Each fluctuation in growth parameters could make the system unstable and directly affect on the crystal quality [9,10]. The temperature gradient adjusted by thermal shields, growth atmosphere and cooling system is the most important growth parameter in the furnace. This parameter influences the crystal perfection by effect on the fluid dynamic and kinetics of a growing crystal [5]. On the other hand, an improper thermal gradient during the growth cause the change of the convexity of solid–liquid interface, reduce/enlarge the size of central core, create large thermal stress and cracks in the crystal [5,9]. The temperature gradient has to be stable during the growth of the crystal. In fact, instability of the temperature gradient leads to increase in the fluctuations of growth rate. Constitutional undercooling may occur due to the fluctuations and cause the change of the morphology of the liquid/solid interface [5,13]. High fluctuations of the water flow rate in the cooling system of growth furnace – wall and induction coil, even for short duration, remarkably affect the growth process of oxide crystals. None of the mentioned references has investigated these fluctuations during the growth process particularly. The aim of the current research is experimental investigation of the effect of intensity and time duration of thermal shocks induced by cooling system on the growth process and crystal quality of Nd:YAG grown by CZ technique [14].

* Corresponding author: Tel.: +381 11 37 13 035; fax: +381 11 31 60 531.
E-mail address: lzorica@yahoo.com (Z.Ž. Lazarević).

http://dx.doi.org/10.1016/j.materresbull.2014.11.033

Owing to the specific characteristics of the method of crystal growth from the high temperature melt (~2273 K) and the required characteristics of a YAG crystal, there are a number of factors that can affect the quality of the resulting crystals: constitutional undercooling, thermal stress, temperature fluctuations and the appearance of the flat crystallization front.

Segregation of impurities that may be present in the starting materials (Y_2O_3), or in the materials added as dopants (Nd_2O_3), can cause a positive gradient of undercooling, leading to the appearance of instability forms of the liquid/solid interface.

The occurrence of constitutional undercooling during the growth of YAG crystals, can lead to the appearance of non-stoichiometry composition of the melt. In this case, the excess of added components also causes segregation and leads to the same effects as in the case of present impurities.

The shape of the liquid/solid interface in crystal growth can have an exceptionally large influence on the crystals properties, and the homogeneous distribution of dopant, strains and dislocation concentration greatly depends on it.

YAG crystal structure is a complex cubic structure containing three different oxygen polyhedral (Fig. 1) [14]. Y^{+3} ions occupy dodecahedral sites and Al^{3+} ions are in octahedral and tetrahedral sites in the ratio of 2:3. This arrangement is the consequence of the differences in the ionic radii: O^{-2}(1.4 Å), Y^{+3}(1.281 Å), Al^{3+}(0.51 Å). Since the ionic radii of Y^{+3} ions and ions of rare-earth are relatively close [11,13,15], trivalent ions of rare earth can replace Y^{+3} ions to a certain small degree. The most frequently used is Nd^{+3} (1.323 Å) ion. For laser gain applications, YAG is typically doped with Nd^{3+} at the 0.2–1.4% atomic weight percent. Lower doped material (0.5–0.8%) is better to steady-state laser performance where optical beam quality is important. Concentration of Nd^{3+} in our samples is, as a common for steady-state laser materials, 0.8 wt.% [16]. It is important to point out that the growth of YAG crystals, which contain Nd^{+3} ions, it is very important coefficient of neodymium in the system $Y_{3-x}Nd_xAl_5O_{12}$ melt – $Y_{3-y}Nd_yAl_5O_{12}$ crystal. Due to the differences in ionic radii between Y^{+3} and Nd^{3+} ions, Nd^{3+} ions are difficult to incorporate into the structure and the coefficient segregation is small, K = 0.2 [17].

In addition, it was noted that the effective coefficient of segregation at a certain rate of rotation is equal to the equilibrium, at a growth temperature i.e., that the growth rate and the rotation does not affect the segregation. In order to obtain the desired concentration of Nd^{3+} ions at the beginning of the crystals, it is necessary that the melt has five times the required concentration of Nd^{3+} ions (K = 0.2). The concentration C_s of Nd^{3+} ions along the crystal change the equation:

$$C_s = KC_{10}(1-y)^{k-1} \quad (1)$$

where is: y-crystallized part, C_{10} – the initial concentration of Nd^{3+} ions in the melt.

During the crystals growth process it is possible, according to the Czochralski's method, to influence the shape of the liquid/solid interface through the growth parameters, such as both the growth and the crystal rotation rate, as well as the temperature gradient. It should be certainly mentioned that growth and rotation rates are rather constant, while the temperature distribution in a melt changes during the process of crystal growth, as the amount of the melt decreases. That gradual reduction of the melts depth, requires the change of the stirring conditions in order to keep stable temperature distribution when lower depths are involved.

Although the seed orientation was , it was noticed that in the initial state of the process of YAG crystal growth, on the liquid/solid interface were formed some (211) and (110) facets. The mechanism of crystal growth can differ depending on whether facets exist on central crystal spots or not. Those spots are characterized by different lattice parameters, thus causing strains in the crystals. The above mentioned reasons require new conditions in which the formation of facets is reduced to the lowest possible degree. Laser rods of high quality can be obtained by cutting crystals large in diameter from those parts that are stress-free. Another approach to this problem involves the establishing of conditions under which the whole liquid/solid interface would be covered by facets. Thus the strains resulting from a difference existing in lattice parameters will be eliminated completely.

To avoid facets formation at the liquid/solid interface it is necessary, according to literature data [18,19], that the rotation rate of a crystal be 150 rpm. But on the other hand such crystals frequently have a high concentration of dislocations.

Other authors are of the opinion [20] that a liquid/solid interface can be completely covered with facets if the rotation rate of a crystal is small (6 rpm). In any case, the rotation rate is not the only factor that has a strong influence on the liquid/solid interface. Such a conclusion can be also made on the basis of the experiments we performed. The most recent investigations (with other crystals) [11,12] proved that a rapid change in the shape of the liquid/solid

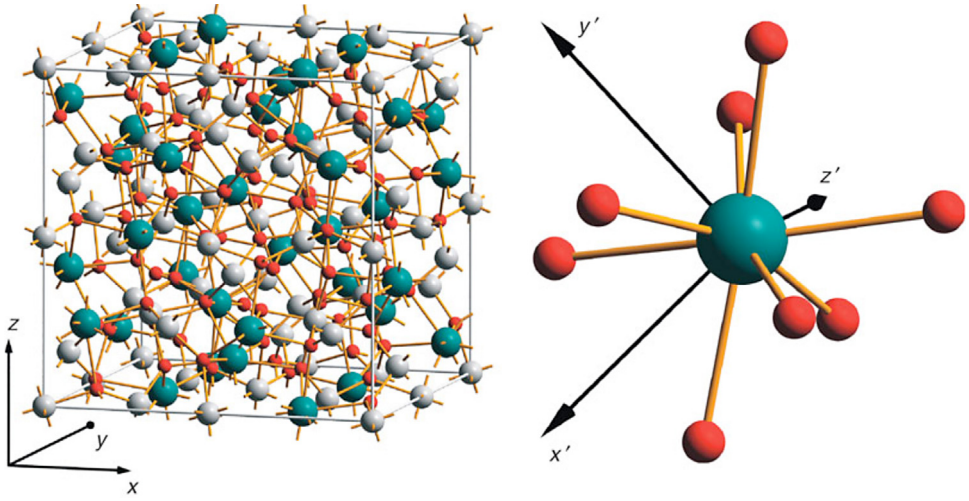

Fig. 1. Unit cell of YAG crystal. Green, white and red sites are occupied by yttrium, aluminium and oxygen, respectively. All together, the unit cell contains eight molecular units $Y_3Al_5O_{12}$. Neodymium occupies yttrium sites substitutionally. The local surrounding of one yttrium site. (For interpretation of the references to color in this figure legend, the reader is referred to the web version of this article.)

interface i.e., inversion, is caused at the very moment when a crystals diameter reaches its critical value for a particular rate of the rotation. This phenomena is the result of changes in the melts movements. At the same time a certain part of a crystal is being remelted and facets are removed. The liquid/solid interface, convex till then, become almost flat with respect to the melt.

Inversion is carried out at the moment when the liquid movements caused by the crystal rotation overcome the natural convexity [21], i.e., when a critical Reynold's number is exceeded. The Reynold's number is as follows:

$$\mathrm{Re} = \frac{\pi \rho D^2 \omega}{2\eta} \tag{2}$$

where is ρ – density of the melt, D – diameter of a crystal, ω – crystal rotation rate and η – viscosity of the melt. Takagi and co-authors [21] established an expression for the diameter of inversion, D_c, which is:

$$D_c = \left(\frac{2}{\pi}\right)^{1/2} \left(\frac{\mathrm{Re}\eta}{\rho}\right)^{1/2} \omega^{-1/2} \tag{3}$$

or

$$D_c \approx \mathrm{K}\omega^{-1/2} \tag{4}$$

This simplified equation is valid only when all parameters of growth remain unchanged. Experimental results show that D_c depends on temperature gradient, growth rate, depth of melt, i.e., diameter of a crucible, and height of meniscus between crystal and melt. D_c grows together with the increase in temperature gradient and decreases with growth rate and rotation. Having used the Grashof's and Reynold's number, Carruthers [22] gave a somewhat more complete equation comprising both the influence of the crucibles dimensions and temperature gradient.

$$D_c = \left(g\alpha\Delta T R^3 \pi^{-2}\right)^{1/4} \omega^{1/2} \tag{5}$$

where is g – gravitation, α – coefficient of thermal expansion of a melt, ΔT – radial difference of temperature in a melt, R – radius of crucible and ω – crystal rotation rate.

Having started from the fact that inversion is determined by Reynold's number, Brice together with Whiffin [23] established the dependence of a critical value $(\mathrm{Re})_c$ on previously mentioned parameters of growth and gave the following equation for the radius of inversion R_c.

$$R_c^2 = \frac{\mathrm{A}G^{1/3}}{\left(1 - R_c^2/R^2\right)\left(1 + \mathrm{B}R_c^2 f\right)} \tag{6}$$

where A and B are constants which are to be experimentally determined, f – growth rate, G – temperature gradient. This equation can be applied only when a melt depth out of which a crystal is pulled, is great. When a melt is shallow the value $(\mathrm{Re})_c$ is higher due to a greater influence of the bottom of the crucible on the mixing process.

In the CZ process, the liquid/solid interface shape is dictated by crystal thermal history. When the interface shape is curved, the thermal field becomes non-uniform along the radial direction, which may result in non-uniformities in mechanical, optical, and electrical properties. Therefore, it is important to keep the interface shape as flat as possible during the single crystal growth. The importance of the interface shape and its role in the single crystal qualities have been emphasized by previous researchers in a review paper published by Dupret and Van Den Bogaert [24]. Control of liquid/solid interface shape is the most important problem in the CZ crystal growth process. Having a high-quality crystal, it is necessary to keep the liquid/solid interface flat or nearly flat which depends on the operating parameters [25]. Numerous research work have been performed to understand the parameters affecting the interface shape and to find out the critical parameters controlling the growth rate at which the interface shape becomes nearly flat. Cockayne et al. [26] determined the interface shape by measuring both the crystal weight and the melt temperature near the interface. They realized that the interface shape is dependent upon the crystal rotation rate. An increase of rotation rate leads to a concave interface with respect to crystal while the convex shape is obtained as a result of low rotation rate. Thus, a lower rotation rate is favorable for obtaining a nearly flat interface. Various researchers studied the effects of different parameters on the shape of crystal interface both numerically and experimentally [27,28]. In almost all these research work, it was found that the rotation rate of the crystal plays a critical role on the liquid/solid interface shape. Kobayashi et al. [29] studied numerically to obtain the critical crystal Reynold's number at which the interface inversion occurs. This phenomenon basically depends on the melt flow structure composed of free and forced convection caused by the crystal rotation rate [30].

The aim of our work was to produce YAG single crystals with and without dopant Nd^{3+} and without a core, the growth parameters and annealing condition investigate, by applying both theoretical and experimental treatment. The structural and optical properties obtained single YAG and Nd:YAG crystals were characterized using XRD, Raman and IR spectroscopy.

2. Experimental

Single YAG and Nd:YAG crystals have been grown using the standard Czochralski technique. Both crystals (Fig. 2) were grown by the Czochralski technique using a MSR 2 crystal puller controlled by a Eurotherm. The atmosphere used was argon. The starting materials were powdered Y_2O_3, Al_2O_3 and Nd_2O_3 (all Koch&Light) all of 4N purity. Powdered ZrO_2 (Koch&Light) of 4N purity was used for isolation. The purity of argon (Tehnogas) was 4N. The iridium crucible (40 mm diameter, 40 mm high) was placed into an alumina vessel surrounded by ZrO_2 wool isolation. Double walls were used to protect the high radiation. To decrease the radial temperature gradient in the melt, alumina was mounted around all the system. The best results were obtained with a pull rate of 2–3 mm h^{-1} for YAG and 1 mm h^{-1} for Nd:YAG crystals

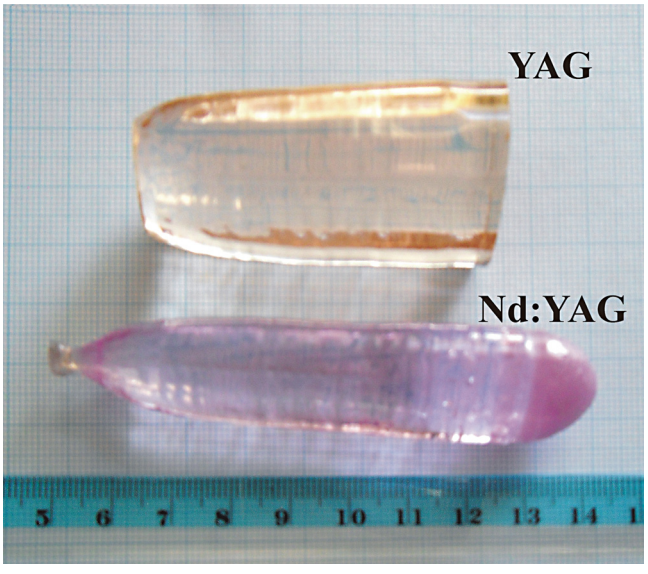

Fig. 2. A view of an obtained: (a) YAG and (b) Nd:YAG single crystals plate.

(Fig. 2). The crystal rotation rates were between 6 and 100 rpm (YAG). The best results were obtained with a crystal rotation of 100 rpm (YAG) and 20 rpm (Nd:YAG). The diameters of crystals were between 10 and 20 mm. The crucible was not rotated during the growth. After the growth run, the crystal boule was cooled at a rate of about 50 K h^{-1} down to room temperature.

Such obtained YAG and Nd:YAG crystals were cut either transversal to the growth axis, or along or parallel to the plane (1 1 0). Then they were polished, smoothed and observed in polarized light.

In order to study the influence of rotation on strains existing in YAG crystal, three series of crystal pulling, of orientation , were performed.

In the first series of experiments, YAG crystals with diameters of about 10 mm were pulled with 3 mm h^{-1} pulling rate. Rotation rate was rapidly changed after a particular crystal length was reached. As with the one crystal, for example, the rotation was changed from 12 to 100 rpm. Within the range of 12–60 rpm no significant influence of rotation on a core has been perceived (Fig. 3). But when the rotation increases to 100 rpm it can be clearly noticed that the core rapidly reduces, and that at that very place some small bubbles appear, while a considerable blurring is noticed.

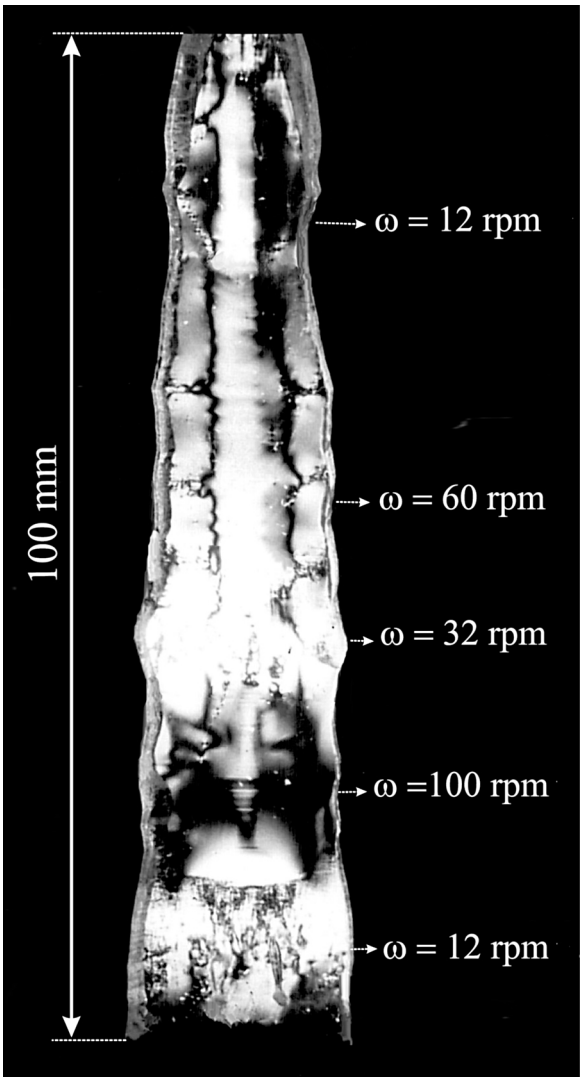

Fig. 3. YAG crystal grown with different rotation rates ω = 12, 60, 32, 100 and 12 rpm.

Rotation of 100 rpm caused melting of the central part of a crystal and a somewhat more rapid growth at the periphery of the same crystal. When rotation is reduced, relative disturbances are far greater as the liquid/solid interface, being almost plain becomes convex with respect to the melt, which causes a rapid increase in growth rate. Similar conclusions can be derived when analyzing the behaviour of other crystals from the same series.

The second group of experiments dealt with crystals, of diameters 15–20 mm, which were pulled at a rate of 2 mm h^{-1}. The rotation during the crystal growth was not changed. Fifteen crystals were pulled with different rotation rates ranging from 6 to 100 rpm.

It can be said on the basis of the results obtained that in crystals rotated at smaller rates (up to 60 rpm) strains, being caused by simultaneous action of two different growth mechanisms, can be noticed (Fig. 4). The core existing in the center of a crystal, which is the result of facet formations, does not essentially depend on rotation rate.The qualitative change appears when a crystal reaches a critical diameter D_c for a particular rotation. The core vanishes under these conditions. It should certainly be pointed out that the core vanishes at the moment when a critical diameter is obtained, but some lesser strains extend along the crystal to a length of about 10 mm. The dependence of type: $D_c = K\omega_c^{-1/2}$ as expected by theoretical postulate, is valid.

In the third series of experiments, the crystals that grew under the same conditions as in second series, were separated from the melt. Thus, we were able to find out immediately the shape of the liquid/solid interface for different rotations and to see the part that was covered with facets. The liquid/solid interface is rather convex with respect to the melt when slow rotations are involved, while it is almost even with faster rotations (90 rpm).

Crystal slices with <111> orientation were cut from the as-grown crystal boule and the slices were subsequently polished on both sides with diamond paste. The mechanically polished slices were chemically polished in liquid H_3PO_4 [15]. Various solutions of H_3PO_4 at different temperatures and for various exposure times were tried for chemical polishing and etching. For chemical polishing, exposure to a concentrated (85%) solution of H_3PO_4 at 603 K (330 °C) for 20 min was confirmed to be suitable. Exposure for 1 h to an 85% solution of H_3PO_4 at 493 K (220 °C) after was found to be a suitable for etching [9,15].

The observations relating to the dislocation were recorded by observing an etched surface of YAG and Nd:YAG crystals, using a Metaval of Carl Zeiss Java metallographic microscope with magnification of 270× and 200×, respectively.

All the obtained crystal YAG plates were observed in polarized light to visualize the presence of a core and/or striations. The absence of a core was confirmed by viewing both polished crystal slices in normal light.

3. Results and discussion

Eq. (5) holds if all other growth parameters are unchanged. Experiments have shown that D_c depends on R,G, melt depth, i.e., the vessel diameter and the meniscus height the crystal and the melt. On the basis of our experimental results it may be concluded that the crystals growing at higher rotation rates, when the inversion of the crystallization front from convex to planar has occurred, do not contain a core and the strains in them are considerably (Figs. 3 and 4).

In the case of YAG crystals with Nd^{3+} ions, after inversion useless crystals with bubbles and opaque regions were obtained. Therefore, investigations were directed at obtaining Nd:YAG crystals with the smallest possible core (1–2 mm).

Investigations that were carried out with YAG not containing Nd^{3+} ions helped us a lot in our studies of YAG containing Nd^{3+} ions.

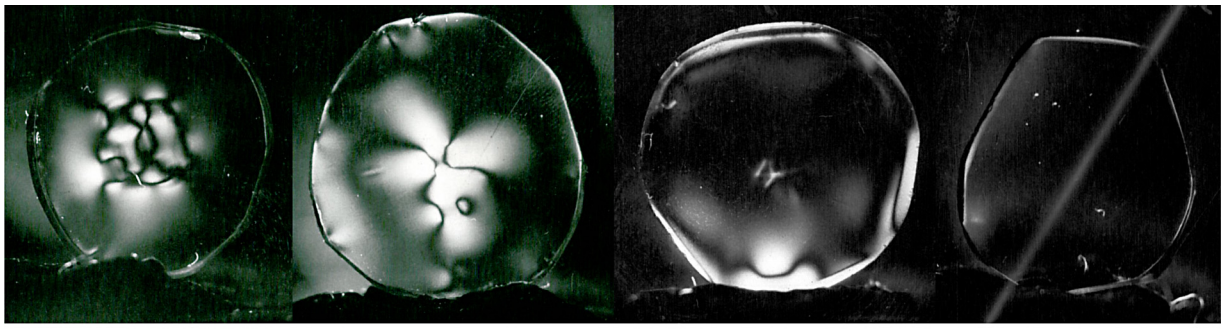

Fig. 4. Cross section of signal YAG crystals grown with different rotation rates under crossed polarizers: (a) 7 rpm, (b) 15 rpm, (c) 60 rpm and (d) 100 rpm.

When investigating YAG containing no Nd^{3+} ions we noticed that after the performed inversion of the liquid/solid interface the crystals obtained did not have cores. On the contrary, when we analyzed YAG containing Nd^{3+} ions we immediately saw that the whole system was far more sensitive, due to the presence of Nd^{3+} ions, to any charge in growth conditions and all our attempts to obtain crystals without a core caused the blurring of the crystals.

In recent years, studies on laser crystals show that YAG crystal has nearly optimal properties that are required of materials for lasers. However, a factor that partially restricts all potential possibilities of this crystal is the difficulty in obtaining single crystals containing a higher concentration of activator (neodymium), while at the same crystal contains all the necessary optical quality. This difficulty is caused by the significant difference of the ionic radii of Nd^{3+} compared to Y^{3+} which in turn makes it difficult to isomorphic substitution of more than 1% (atomic) Nd^{3+} in YAG crystal. Therefore, many studies in order to obtain Nd:YAG crystals oriented in the direction of getting other elements (for example lutenium – Lu), whose ionic radius much smaller than Y^{3+}, so their embedding in the crystal lattice of YAG achieves the effect of compensation between such ions and ions Nd^{3+} and crystal lattice parameter remains approximately 12.01 Å. The main defects of the crystal structure, not counting dislocations, which are the proper conduct of the process of crystal growth may keep a level of 100 dislocations per cm^2 are also inhomogeneous incorporation of Nd^{3+} due to the appearance of (2 1 1) flat in the center of the crystal orientation (1 1 1) zone of the stress in the direction (1 1 0) on the plane (1 1 1) and furrows caused by impurity character of the interface crystal-melt during the process of crystal growth. From the Fig. 5 it can be observed dislocations on YAG and Nd^{3+}:YAG single crystals, respectively. Etch pits have the shape of a three-sided pyramid. Number of dislocations is of the order of 10^4 per cm^2. Most of the crystals were no dislocation.

The works of the oxide crystal material have shown that thermal stress in the crystal, which may be cooled to cause the occurrence of dislocations. These errors reduce the crystallographic and optical perfection of the crystals. Their occurrence can be prevented by using an annealing which thermal stresses can be limited to values that are lower than the limits of the critical stress for a given crystal. The occurrence of flat at the front of crystallization leads to the appearance of stress in a crystal YAG and also uneven incorporation of Nd^{+3} ions. Fluctuations in temperature cause a change in the growth rate which leads to stress in the crystals and uneven incorporation of Nd^{+3} ions. Tests in polarized light showed that the index of refraction in the crystal YAG we received has not the same value of the cross section. Difference in refractive index are due to the crystallization front partially covered with a flatbed and partly not.

The mechanism of the crystal growth is not the same when it is growing with a flat surface (flat across) rise than when roughened surface. This leads to the crystal have parts that have different lattice parameters, the local saturation with oxygen vacancies. Removal of stress annealing may be performed in argon, to the air, in vacuum and the oxidation atmosphere [15,17,31]. Since the transition from brittle to ductile state in YAG at 1350 °C, annealing, we performed in 1600, 1700 and 1800 °C. Annealing was performed in the same unit in which they are drawn crystals. The average speed of raising and lowering the temperature ranged from 1 to

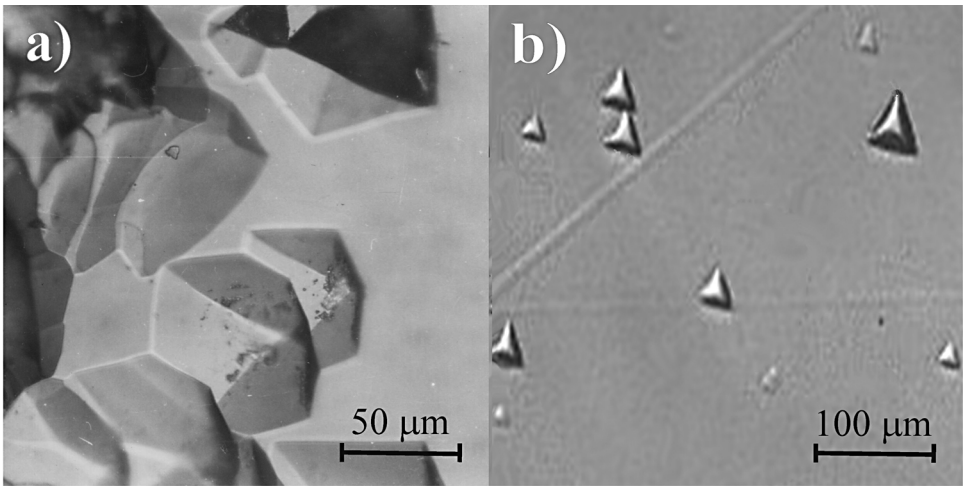

Fig. 5. The microscopic image of the surface YAG Nd:YAG single crystals plate etched with H_3PO_4 in the direction (1 1 1). Magnification of 270× and 200×, respectively.

1.5 °C min^{-1}. After annealing was done observing the polarized light. Based on the obtained data, it was concluded that prolonged heating at 1800 °C able to mitigate the difference in refractive index. When testing centers scattering of light we concluded that if the crystal pull rate of 0.9 mm h^{-1} there is no scattering centers. At speeds of 1–1.3 mm h^{-1} is little shimmer, while at higher speeds shimmer is more intense (refers to Nd: YAG).

The existence of centers of scattering of light due to the presence of very small bubbles, inclusions, etc., in the obtained crystals was carried out using a He–Nd laser beam. Number of dislocation is very small. Frequently there are none. Mosaic blocks were not detected.

3.1. Structural and spectroscopic characterization

The structural properties were obtained using X-ray diffraction analysis of powdered single crystal samples. The X-ray diffraction (XRD) curves for powdered YAG and Nd:YAG is shown in Fig. 6. Diffractions correspond to JCPDS 79-1892. The unit cell of YAG and Nd:YAG is calculated by the least square method using 15 reflections. In Fig. 6, all the reflections correspond to YAG crystals and not any other phase was found. The calculated result reveals that the crystals have body-centered cubic Bravais lattice with space group Ia3d. The lattice parameter for YAG is a = 11.9538 Å, and for Nd:YAG a = 11.9677 Å, what is slightly less than the published data [9,17] (12.011 Å). The cell parameter of Nd:YAG crystal is 0.12% larger than that of YAG crystal. The radius of Nd^{3+} ion (1.249 Å) is larger than the radius of Y^{3+} ion (1.159 Å), and the difference of about 7.8% not only makes the incorporation of Nd^{3+} into the Y^{3+} site of the crystal lattice hard, but also results in larger cell parameter. It causes a shift of diffractions in the spectra of Nd:YAG towards smaller 2θ – angles. Obtained differences are presented in Table 1.

The FWHM of [1 1 1] symmetric rocking curve measured by X-ray double-crystal diffractometry is equal to 0.5183. Compared with research of Chani by Czochralski method (FWHM = 0.381°) [32] and Zhang by the horizontal directional solidification – HDS method (FWHM = 0.2631°) [17], the value of FWHM demonstrates the good crystallinity of the Nd:YAG crystal.

The large number of atoms in the primitive cell leads to 240 (3×80) possible normal modes which can be classified according to the irreducible representation of the O_h group as follows: $3A_{1g} + 5A_{2g} + 8E_g + 14T_{1g} + 14T_{2g} + 5A_{1u} + 5A_{2u} + 10E_u + 18T_{1u} + 16T_{2u}$. The 25 modes having symmetries A_{1g}, E_g, and T_{2g} are Raman active while the 18 having T_{1u} symmetry are IR active [33–35]. The 16 of the 25 Raman active vibrational modes can be observed in the Raman spectrum from 100 to 900 cm^{-1}. The Raman spectrum of rare earth doped YAG compounds can be divided into two different parts: the high frequency region (500–900 cm^{-1}) and the low frequency region (<500 cm^{-1}). The high frequency region accounts to the ν_1 (breathing mode), ν_2 (quadruple) and ν_4 molecular internal modes associated with the (AlO_4) group, whilst the low frequency region is due to: (i) translational motion of the rare earth ions, (ii) rotational and translational motion of the AlO_4 units, and (iii) the ν_3 molecular mode of the AlO_4 [33,34].

The Raman spectra of YAG and Nd:YAG single crystals have been recorded in 100–900 cm^{-1} spectral range at room temperature (Fig. 7). The differences in the Raman spectra of the pure YAG crystal and Nd^{3+} doped YAG crystal are in slightly blue shifting of modes in doped crystal, Table 2, and in the shape of some peaks, also. It is observable that some peaks show a doublet structure, and that some weak modes in the low energy side of regular modes

Table 1
Positions of the diffractions observed in XRD spectra of YAG and Nd:YAG powder and their mutual difference (Δ) caused by doping.

(*hkl*)	YAG 2θ(°)	Nd:YAG 2θ(°)	Δ (°)
−211	18.139	17.99	0.149
−220	21.03	20.81	0.22
−321	27.876	27.75	0.126
−400	29.916	29.68	0.236
−420	33.475	33.367	0.108
−422	36.774	36.65	0.124
−431	38.393	38.222	0.171
−521	41.333	41.155	0.178
−440	42.712	42.69	0.022
−611	46.831	46.6	0.231
−541	–	49.455	–
−631	51.83	51.67	0.16
−444	52.989	52.74	0.249
−640	55.379	55.167	0.212
−552	56.528	56.322	0.206
−642	57.868	57.454	0.414
−651	60.947	60.75	0.197
−800	61.9	61.77	0.13
−820	–	64.055	–
−660	66.146	65.97	0.176
−743	67.426	–	–
−840	70.285	70.023	0.262
−842	72.324	72.078	0.246
−655	73.29	73.09	0.2
−664	74.385	74.056	0.329
−932	77.143	76.949	0.194
−844	–	79.122	–
	a (Å)	a(Å)	
	11.9538	11.9677	

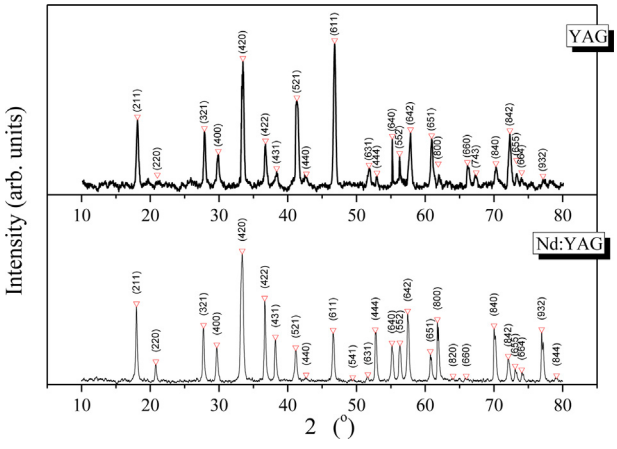

Fig. 6. X-ray diffraction patterns of the: (a) YAG and (b) Nd^{3+}:YAG powdered sample.

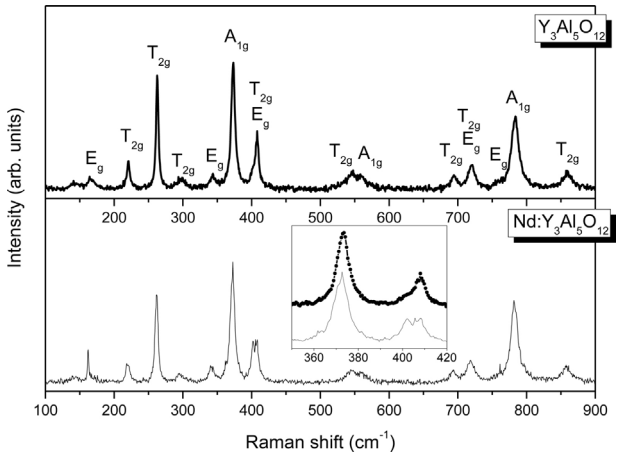

Fig. 7. Raman spectra of YAG and Nd:YAG single crystals at room temperature.

Table 2
Position (cm^{-1}) of the modes in the Raman spectra and symmetries of lines of YAG Nd:YAG single crystals.

Symmetry type	Experimental frequency (cm^{-1})		Vibrations
	YAG	Nd:YAG	
E_g	164	162	Y or Nd
T_{2g}	219	221	Translation
T_{2g}	263	263	Translation + Rotation + $\nu_3(AlO_4)$
T_{2g}	294	295	
E_g	340	343	
A_{1g}	373	373	
T_{2g}	403	409	
E_g	–	407	
T_{2g}	544	548	ν_2 (AlO_4)
A_{1g}	556	557	
T_{2g}	690	693	$\nu_1 + \nu_4$ (AlO_4)
E_g	720	720	
T_{2g}	720	720	
A_{1g}	784	783	
T_{2g}	857	858	

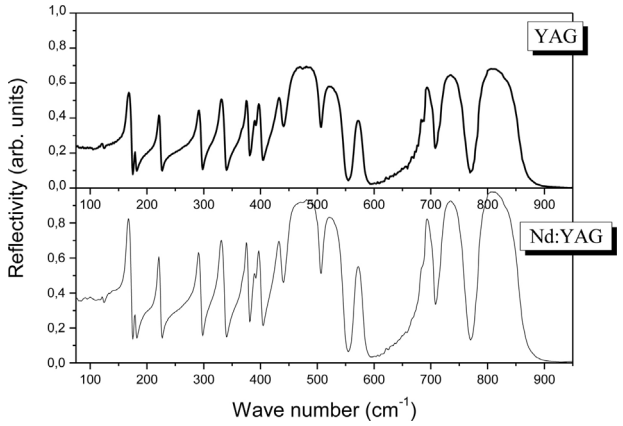

Fig. 8. IR reflectance spectra of YAG and Nd:YAG single crystals at room temperature.

become visible, Fig. 7, insert. These new features in the Raman spectra are not a consequence of increasing disorder, but indicate a regular substituting of Y^{3+} by heavier Nd^{3+}-ions.

According to work by Su et al., on Nd:YAG [36], the peaks at 161, 219, 263, 340, 373, 402 and 407 cm^{-1} (Fig. 7 and Table 2) have been attributed to the translatory motion of the Y^{3+} or Nd^{3+}-ions within the distorted cube with eight oxygen ions at the corners, and also the heavy mixing of the translational, rotational, and ν_3 mode of the (AlO_4) unit. The vibrational modes at 543 and 556 cm^{-1} can be assigned as the ν_2 mode of the (AlO_4) unit. These peaks are the internal stretching vibrations (ν_1 and ν_4) between aluminum ions and oxygen in the tetrahedral (AlO_4) unit.

The Nd^{3+} ions substitute for Y^{3+} in YAG without the need for charge compensation. The larger size of the Nd^{3+} ions results in polyhedral with sides that are greater than those in Al^{3+} polyhedral. That distorts the lattice and thus limits the maximum doping concentration a few atomic weight percent. Concentration of Nd^{3+} in our samples is, as a common for laser materials, 0.8 wt.%. The lattice strains that are introduced by doping affect the properties of the optical spectra.

The reflectivity spectra of YAG and Nd:YAG single crystals were recorded in far-IR and mid-IR region at room temperature (298 K). The IR reflectance spectra of these crystals are shown in Fig. 8. The seventeen of $18T_{1u}$ IR-active modes are visible in the near normal reflectivity spectra of YAG and Nd:YAG crystals, Fig. 8. There are strong metal oxygen vibrations in region 650–800 cm^{-1} which are characteristics of Al—O bond: peaks at 784/854, 719/763 and 691/707 cm^{-1} correspond to asymmetric stretching vibrations in tetrahedral arrangement. Peaks at 566/582, 510/547 and 477/505 cm^{-1} are asymmetric stretching vibrations and 453/483 cm^{-1} is symmetric vibration of Al—O bond in octahedral arrangement of garnet structure. Lower energy peaks correspond to translation and vibration of cations in different coordination – tetrahedral, octahedral and dodecahedral in the case of four lowest modes (Table 3) [37].

Graphical presentation of the Kramers–Krönig analysis shows that with doping of YAG with Nd^{3+}, TO modes undergo a red shift of 1–3 cm^{-1}, what is expected because of greater atomic mass of neodymium (144.2) related to yttrium (88.9) (Fig. 9). The values of these modes are presented in Table 3.

Table 3
Parameters of fit the IR spectra of YAG and Nd:YAG single crystals and the transverse (TO) and the longitudinal (LO) frequencies values obtained from Kramers–Krönig analysis (peak positions ε_2 and σ).

YAG TO/LO wave number (cm^{-1})	Nd:YAG TO wave number (cm^{-1})	Vibrations
122/122.6	122	$T(+T_d)$ transl. of tetr. and dodecah. cation
165/173	163	T_d transl. of dodecah. cation
180/180	178	$T_d(+T)$ transl. of tetr. and dodecah. cation
221/225	219	T_d transl. of dodecah. cation (translations of cations in YO_3 and AlO_4)
291/296	289	T_0
327/338	328	T transl of tetrah. cation
375/380	374	R libr. of tetrah.
390/392	389	T_0 transl. of octah.
396/402	395	R libr. of tetrah.
432/438	431	T_0 transl. of octah. (translations + libration of cations in AlO_6 and AlO_4)
453/483	449	ν_2 symmetric
477/505	475	ν_4 symmetric
510/547	509	ν_4
566/582	595	ν_4 (symmetric and asymmetric stretching of Al–O in octahedrons)
691/707	690	ν_3
719/763	717	ν_3
784/854	783	ν_3 (asymmetric stretching of Al–O in tetrahedrons)

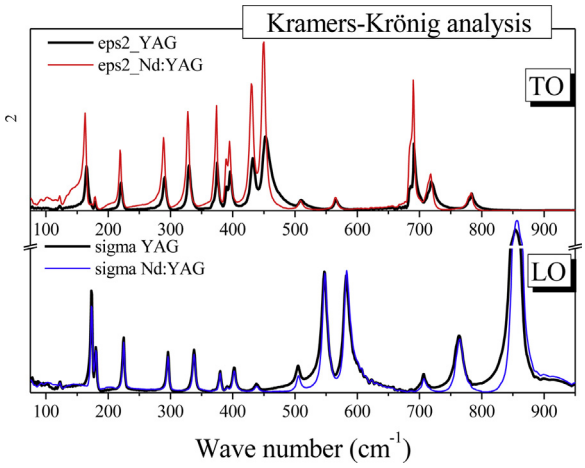

Fig. 9. TO and LO modes of YAG and Nd:YAG single crystals obtained by the Kramers–Krönig analysis.

4. Conclusions

In this paper, we used the Czochralski method to obtain good quality YAG and Nd:YAG crystals. The investigations were based on the growth mechanisms and the shape of the liquid/solid interface on the crystal properties and incorporation of Nd^{3+} ions. The obtained single YAG and Nd:YAG crystals were studied by use of X-ray diffraction, Raman and IR spectroscopy. There are strong metal oxygen vibrations in region 650–800 cm^{-1} which are characteristics of Al—O bond: peaks at 784/854, 719/763 and 691/707 cm^{-1} correspond to asymmetric stretching vibrations in tetrahedral arrangement. Peaks at 566/582, 510/547 and 477/505 cm^{-1} are asymmetric stretching vibrations and 453/483 cm^{-1} is symmetric vibration of Al—O bond in octahedral arrangement of garnet structure. Lower energy peaks correspond to translation and libration of cations in different coordinations – tetrahedral, octahedral and dodecahedral in the case of the lowest modes.

Acknowledgments

This research was financially supported by the Ministry of Education, Science and Technological Development of the Republic of Serbia through Project No. III45003.

References

[1] D. Jun, D. Peizhen, X. Jun, J. Cryst. Growth 203 (1999) 163–167.
[2] A.K. Pradhan, K. Zhang, G.B. Loutts, Mater. Res. Bull. 39 (2004) 1291–1298.
[3] M. Yadegari, M. Asadian, H. Saeedi, Y. Khodaei, N. Mirzaei, J. Cryst. Growth 367 (2013) 57–61.
[4] M. Katsurayama, Y. Anzai, A. Sugiyama, M. Kokie, Y. Kato, J. Cryst. Growth 229 (2001) 193–198.
[5] H. Saeedi, M. Yadegari, S. Enayati, M. Asadian, M. Shojaee, Y. Khodaei, N. Mirzaei, I. Mashayekhi Asl, J. Cryst. Growth 363 (2013) 171–175.
[6] M.H. Tavakoli, E. Mohammad-Manesh, S. Omid, Cryst. Res. Technol. 45 (2010) 1117–1122.
[7] C. Belouet, J. Cryst. Growth 15 (1972) 188–194.
[8] J.H. Mun, A. Novoselov, A. Yoshikawa, G. Boulon, T. Fukuda, Mater. Res. Bull. 40 (2005) 1235–1243.
[9] A. Golubovic, S. Nikolic, R. Gajic, S. Djuric, A. Valcic, J. Serb. Chem. Soc. 67 (2002) 291–300.
[10] H. Saeedi, M. Asadian, Sh. Enayati, N. Mirzaei, Cryst. Res. Techn. 46 (2011) 1229–1234.
[11] Z.Ž. Lazarević, P. Mihailović, S. Kostić, M.J. Romčević, M. Mitrić, S. Petričević, J. Radunović, M. Petrović-Damjanović, M. Gilić, N.Ž. Romčević, Opt. Mater. 34 (2012) 1849–1859.
[12] Z. Lazarević, S. Kostić, V. Radojević, M. Romčević, M. Gilić, M. Petrović-Damjanović, N. Romčević, Physica Scripta T157 (2013) 14046.
[13] E. Kanchanavaleerat, D. Cochet-Muchy, M. Kokta, J. Stone-Sundberg, Opt. Mater. 26 (2004) 337–341.
[14] R. Kolesov, K. Xia, R. Reuter, R. Stöhr, A. Zappe, J. Meijer, P.R. Hemmer, J. Wrachtrup, Nat. Commun. 3 (2012) 1029, doi:http://dx.doi.org/10.1038/ncomms2034.
[15] Y. Peizhi, D. Peiyhen, Y. Yhiwen, T. Yulian, J. Cryst. Growth 218 (2000) 87–92.
[16] A. Golubovic, S. Nikolic, R. Gajic, Z. Dohcevic-Mitrovic, A. Valcic, Metalurgija 10 (2004) 363–370.
[17] M. Zhang, H. Guo, J. Han, H. Zhang, C. Xu, J. Cryst. Growth 340 (2012) 130–134.
[18] B. Cockayne, J.M. Roslington, A.W. Vere, J. Mater. Sci. 8 (1973) 382–384.
[19] B. Cockayne, J. Cryst. Growth 3–4 (1968) 60–70.
[20] C. Belouet, J. Cryst. Growth 15 (1972) 188–194.
[21] K. Takagi, T. Fukazawa, M. Ishii, J. Cryst. Growth 32 (1976) 89–94.
[22] J.R. Carruthers, J. Cryst. Growth 36 (1976) 212–214.
[23] J.C. Brice, P.A.C. Whiffin, J. Cryst. Growth 38 (1977) 245–248.
[24] F. Dupret, N. Van den Bogaert, in: D.T.J. Hurle (Ed.), Handbook of Crystal Growth, Elsevier, North-Holland, Amsterdam, 1994, pp. 875.
[25] P.W. Mokruchnikov, Cryst. Res. Technol. 34 (1999) 1169–1173.
[26] B. Cockayne, B. Lent, J.M. Roslington, J. Mater. Sci. 11 (1976) 259–263.
[27] J.H. Jeong, I.S. Kang, J. Cryst. Growth 218 (2000) 294–312.
[28] A. Hirata, M. Tachibana, Y. Okano, T. Fukuda, J. Cryst. Growth 128 (1993) 195–200.
[29] M. Kobayashi, T. Tsukada, M. Hozawa, J. Cryst. Growth 180 (1997) 157–166.
[30] M. Asadian, S.H. Seyedein, M.R. Aboutalebi, A. Maroosi, J. Cryst. Growth 311 (2009) 342–348.
[31] M. Świrkowicz, M. Skórczakowski, J. Jabczyński, A. Bajor, E. Tymicki, B. Kaczmarek, T. Lukasiewicz, Opto-Electron. Rev. 13 (2005) 213–220.
[32] V.L. Chani, A. Yoshikawa, Y. Kuwano, J. Cryst. Growth 204 (1999) 155–162.
[33] J.P. Hurrell, P.S. Porto, I.F. Chang, S. Mitra, R.P. Bauman, Phys. Rev. 173 (1965) 173–851.
[34] Y.F. Chen, P.K. Lim, S.J. Lim, Y.J. Yang, L.J. Hu, H.P. Chiang, W.S. Tse, J. Raman Spectrosc. 34 (2003) 882–885.
[35] A. Lukowiak, R.J. Wiglusz, M. Maczka, P. Gluchowski, W. Strek, Chem. Phys. Lett. 494 (2010) 279–283.
[36] J. Su, Q. Zhang, S. Yin, D. Sun, S. Shao, Spectrosc. Spect. Anal. 29 (2009) 1577–1580.
[37] A.M. Hofmeister, K.R. Campbell, J. Appl. Phys. 72 (1992) 638–646.